# Noninvasive imaging of cell proliferation following mitogenic extracellular kinase inhibition by PD0325901

**Julius Leyton,[1] Graham Smith,[1] Mark Lees,[1] Meg Perumal,[1] Quang-de Nguyen,[1] Franklin I. Aigbirhio,[2] Oksana Golovko,[2] Quimin He,[3] Paul Workman,[4] and Eric O. Aboagye[1]**

[1]Molecular Therapy Group, Faculty of Medicine, Imperial College London, Hammersmith Hospital, London, United Kingdom; [2]Wolfson Brain Imaging Centre, University of Cambridge, Addenbrookes Hospital, Cambridge, United Kingdom; [3]Department of Oncology, Clinical Research Laboratory, Huddinge University Hospital, Karolinska Institute, Stockholm, Sweden; and [4]Cancer Research UK, Centre for Cancer Therapeutics, The Institute of Cancer Research, Sutton, Surrey, United Kingdom

## Abstract

**The mitogenic extracellular kinase 1/2 (MEK1/2) inhibitor, PD0325901, has potent activity in a number of cancer cell types *in vitro*. In SKMEL-28 human melanoma cells (*BRAF* mutant), the drug rapidly decreased phosphorylated extracellular signal-regulated kinase 1/2, cyclin D1, and thymidine kinase 1 protein levels. We investigated if 3′-deoxy-3′-[$^{18}$F]fluorothymidine-positron emission tomography ([$^{18}$F]FLT-PET) could be used to image changes in cell proliferation following MEK1/2 inhibition *in vivo*. Mice bearing SKMEL-28 and human colon cancer HCT116 (*K-RAS* mutant) xenografts were treated daily with PD0325901 at 25 mg/kg and imaged by dynamic [$^{18}$F]FLT-PET after 1 and 10 days of initiating treatment. The drug decreased tumor [$^{18}$F]FLT uptake after 1 and 10 days of treatment compared with control animals. The normalized (maximal) [$^{18}$F]FLT uptake in SKMEL-28 xenografts (at 60 minutes; $NUV_{max}$) after 1 day of vehicle or PD0325901 therapy was 1.81 ± 0.18 versus 1.23 ± 0.10, respectively ($P = 0.03$). In this model, $NUV_{max}$ after 10 days was 2.07 ± 0.40 versus 1.08 ± 0.14, respectively ($P = 0.03$). The corresponding values for HCT116 tumors were 2.30 ± 0.84 versus 1.88 ± 0.36 ($P = 0.045$) after 1 day, and 1.97 ± 0.13 versus 1.00 ± 0.03 ($P = 0.03$) after 10 days. Similar changes were found for other [$^{18}$F]FLT retention variables. The drug decreased phosphorylated extracellular signal-regulated kinase 1/2, cyclin D1, and thymidine kinase 1 protein. Tumor [$^{18}$F]FLT-PET variables correlated with proliferation as measured by Ki67 labeling index ($r \geq 0.6$; $P \geq 0.003$). In summary, [$^{18}$F]FLT-PET is a sensitive imaging biomarker for detecting the antiproliferative effect of MEK1/2 inhibition by PD0325901. [Mol Cancer Ther 2008;7(9):3112–21]**

## Introduction

The mitogen-activated protein kinase (MAPK) pathway involving RAS, RAF, mitogenic extracellular kinase (MEK1/2), and extracellular signal-regulated kinase (ERK) regulate cell proliferation, survival, and differentiation in response to extracellular signals. The pathway is activated in several cancers with overall mutation rates of ~15% to 30% for *RAS* (1) and ~7% for *BRAF* (2). In human melanoma, *BRAF* mutations occur in ~66% of cases (2), with the most common mutation being a glutamic acid for valine substitution at position 600 (V600E). This substitution, by mimicking phosphorylation of the activation segment, activates *BRAF* ~500-fold and stimulates constitutive MAPK activity (3). In colorectal cancer, *K-RAS* mutations occur in ~27% of cases (4). The MAPK pathway is therefore a key target for therapeutic intervention. MEK1/2 has no reported oncogenic properties but serves as a central axis for this pathway.

A number of drugs, including CI-1040, PD0325901, and AZD6244 have been developed to target MEK1/2 (5–9). Activating mutations in *BRAF* and *RAS* have been shown to sensitize cells to these MEK1/2 inhibitors (6, 9), but clinical response is not limited to tumors harboring such mutations (5). Furthermore, all these inhibitors have been shown to reduce levels of phosphorylated ERK1/2 (pERK1/2) in cells *in vitro* or in tumor biopsies (5–9), although the best clinical response observed has been stable disease (5, 7, 8). These findings indicate that reduction in pERK1/2 does not necessarily predict growth inhibition. Cell proliferation has been proposed as a useful biomarker of MEK1/2 inhibition (10). Clearly, assessment of cell proliferation by imaging will be more desirable than multiple biopsy methods. In the present study, we examined the relationship between imaging variables derived from 3′-deoxy-3′-[$^{18}$F]fluorothymidine-positron emission tomography ([$^{18}$F]FLT-PET) and cognate biochemical effects of the MEK1/2 inhibitor PD0325901 (9). [$^{18}$F]FLT-PET measures thymidine kinase 1 (TK1) activity *in vivo* (11, 12). A decrease in the activities of $G_1$ phase cyclins and retinoblastoma hypophosphorylation regulate TK1 mRNA and protein, leading to decreases in [$^{18}$F]FLT uptake (13). Efficacious doses of cytotoxic drugs and gene

Received 3/26/08; revised 5/21/08; accepted 6/10/08.

**Grant support:** Program grants from Cancer Research UK (C2536/A5708) and United Kingdom Medical Research Council (U.1200.02.005.00001.01).

The costs of publication of this article were defrayed in part by the payment of page charges. This article must therefore be hereby marked *advertisement* in accordance with 18 U.S.C. Section 1734 solely to indicate this fact.

**Requests for reprints:** Eric O. Aboagye, Imperial College London Faculty of Medicine, Room 240 MRC Cyclotron Building, Hammersmith Hospital, Du Cane Road, London W12 ONN, United Kingdom, Phone: 44-208-383-3759; Fax: 44-208-383-1783. E-mail: eric.aboagye@imperial.ac.uk



doi:10.1158/1535-7163.MCT-08-0264

therapies also induce reductions in tumor [$^{18}$F]FLT uptake (14, 15). Indeed, Solit and coworkers have recently shown the advantage of [$^{18}$F]FLT-PET over [$^{18}$F]fluorodeoxyglucose-PET for monitoring the therapeutic response to PD0325901 (16). However, dynamic imaging was not done in that study; therefore, the value of different imaging variables and their relationship(s) to proliferation signals were not established. Prior to *in vivo* studies with PD0325901, we established the time course of drug effect in a sensitive cell line (SKMEL-28) *in vitro*. The potential of different [$^{18}$F]FLT-PET variables as downstream pharmacodynamic imaging end points of growth inhibition following MEK1/2 inhibition was then assessed in two human tumor xenograft models—SKMEL-28 melanoma and HCT116 colorectal cancer.

## Materials and Methods

### Radiopharmaceuticals and Drug

[$^{18}$F]FLT was synthesized by radiofluorination of the 3-*N*-boc-5′-*O*-dimethoxytrityl-3′-*O*-nosyl-thymidine precursor using a GE TracerLab MX synthesis module (GE Healthcare UK Limited) based on a previously described method (17). All samples had >98% radiochemical purity as determined by high-performance liquid chromatography with radiochemical detection, and the specific radioactivity was 120 to 150 GBq/μmol at the end of the synthesis. PD0325901 (*N*-[(*R*)-2,3-dihydroxy-propoxy]-3,4-difluoro-2-[2-fluoro-4-iodo-phenylamino]-benzamide) was obtained from the Division of Signal Transduction Therapy, University of Dundee, Dundee, Scotland.

### Cell Culture and Treatment

SKMEL-28 and HCT116 cells were cultured in RPMI 1640 growth medium containing 10% (v/v) fetal bovine serum, 2 mmol/L of L-glutamine, 100 units/mL of penicillin, and 100 g/mL of streptomycin and grown in a 5% $CO_2$ incubator at 37°C. Cells in exponential growth were used for subsequent studies. To examine the effect of PD0325901 *in vitro* on SKMEL-28 cells, the growth medium was replaced with medium containing 1 μmol/L of PD0325901 or DMSO (the final concentration of DMSO in both cases was 0.1%). The plates were then incubated for 0.5, 2, 4, 24, or 48 hours and harvested.

### Protein Analysis

The levels of pERK1/2, total ERK1/2, cyclin D1, TK1, pAKT, total AKT, cleaved caspase-3 (Asp$^{175}$), and β-actin (loading control) protein were determined by Western blot analysis. In addition, Western blot analyses were also done on excised frozen tumor material. For this, SKMEL-28 and HCT116 tumors (after imaging studies) were snap-frozen in liquid nitrogen and stored at −80°C until analysis. The tumors were pulverized in liquid nitrogen and homogenized in 100 μL of ice-cold triple detergent buffer [50 mmol/L Tris-HCl (pH 8.0), 150 nmol/L NaCl, 0.02% sodium azide, 0.1% SDS, 1% NP40, 0.5% sodium deoxycholate, and 10 μL/mL protease inhibitor mixture]. Lysates were clarified by centrifugation (15,000 × *g* for 10 min at 4°C) and the supernatants were analyzed for total protein content using a commercial bicinchoninic acid protein assay kit (Perbio Science). Aliquots of the supernatant (containing 30 μg of protein) were assayed as previously reported (13).

The primary antibodies used in this study included the following: rabbit polyclonal anti-phosphorylated p44/42 MAPK (Thr$^{202}$/Tyr$^{204}$) antibody (1:1,000), rabbit polyclonal anti-total p44/42 MAPK antibody (1:1,000 dilution), rabbit polyclonal anti–cyclin D1 antibody (1:1,000), mouse biotinylated monoclonal anti-TK1 (no. 1-8-5:4-1D11, 1:20,000 dilution; Svanova Biotech), rabbit polyclonal antiphosphorylated pAKT and rabbit polyclonal anti-total AKT (Cell Signaling Technology), cleaved caspase-3 (Asp$^{175}$), and mouse polyclonal anti–β-actin (1:2,000; Santa Cruz Biotechnology). The membranes were processed and bands were quantified as previously reported (13). Four tumor samples were analyzed from each of the control and treatment groups.

### Determination of mRNA Levels by Quantitative Real-time PCR

The effect of 1 μmol/L of PD0325901 on the transcription of a number of candidate genes was assessed in SKMEL-28 cells. Cells were washed and RNA from the cells was extracted with Trizol (Invitrogen Life Technologies) as per the manufacturer's instructions with a slight modification in that the aqueous phase was cleaned up with chloroform/isoamyl alcohol mixture (24:1).

The cDNA generated was used as a template in real-time PCR reactions with a SYBR-Green PCR master mix (Applied Biosystems). All amplification reactions were done in triplicate using 96-well optical reaction plates (MicroAmp, Applied Biosystems) on an Applied Biosystem 7500 Fast System. The results were then normalized to the housekeeping gene *HPRT* and expressed as a ratio. The primers were designed from the literature or from the GenBank Ensembl sequence. The sequences were assessed for species-specificity by a BLAST search.[5] Where possible, primers were designed to cover putative introns. Dissociation curves were done after each PCR run to ensure that a single PCR product had been amplified. The products were also analyzed by gel electrophoresis and sequencing on a primer pair to ensure that the correct gene fragment was amplified. Levels of the PCR-amplified *HPRT* were found to be constant for all the treatment groups, indicating suitability for use as a control (data not shown). The PCR primers (Supplementary Table S1)[6] were synthesized by Sigma-Genosys.

### Determination of ATP Levels

Because [$^{18}$F]FLT uptake is dependent not just on TK1, but also ATP (11), we examined the effect of PD0325901 on ATP in tumor samples. ATP levels were determined by a bioluminescence assay (ENLITEN ATP assay system; Promega) as previously reported (13).

[5] http://www.ncbi.nlm.nih.gov

[6] Supplementary material for this article is available at Molecular Cancer Therapeutics Online (http://mct.aacrjournals.org/).

### Tumor Models and Drug Treatment

All experiments were done by licensed investigators in accordance with the United Kingdom Home Office's regulations under the Animal (Scientific Procedures) Act 1986 and were within guidelines set out by the United Kingdom Coordinating Committee for Cancer Research's Ad hoc Committee on the Welfare of Animals in Experimental Neoplasia (18). We used two xenograft models to assess the biological activity of PD0325901, i.e., human melanoma SKMEL-28 and human colon carcinoma HCT116 xenografts. Six- to 8-week-old BALB/c *nu/nu* mice were obtained from Harlan United Kingdom, Ltd., and tumors were induced by s.c. inoculation of $5 \times 10^6$ SKMEL-28 cells (*BRAF* mutant) or HCT116 cells (*K-RAS* mutant) on the back of the mice. SKMEL-28 cells were prepared as a suspension in 25% of growth medium in basement membrane matrix (BD Matrigel; BD Bioscience); HCT116 cells were prepared in PBS. Tumor dimensions were

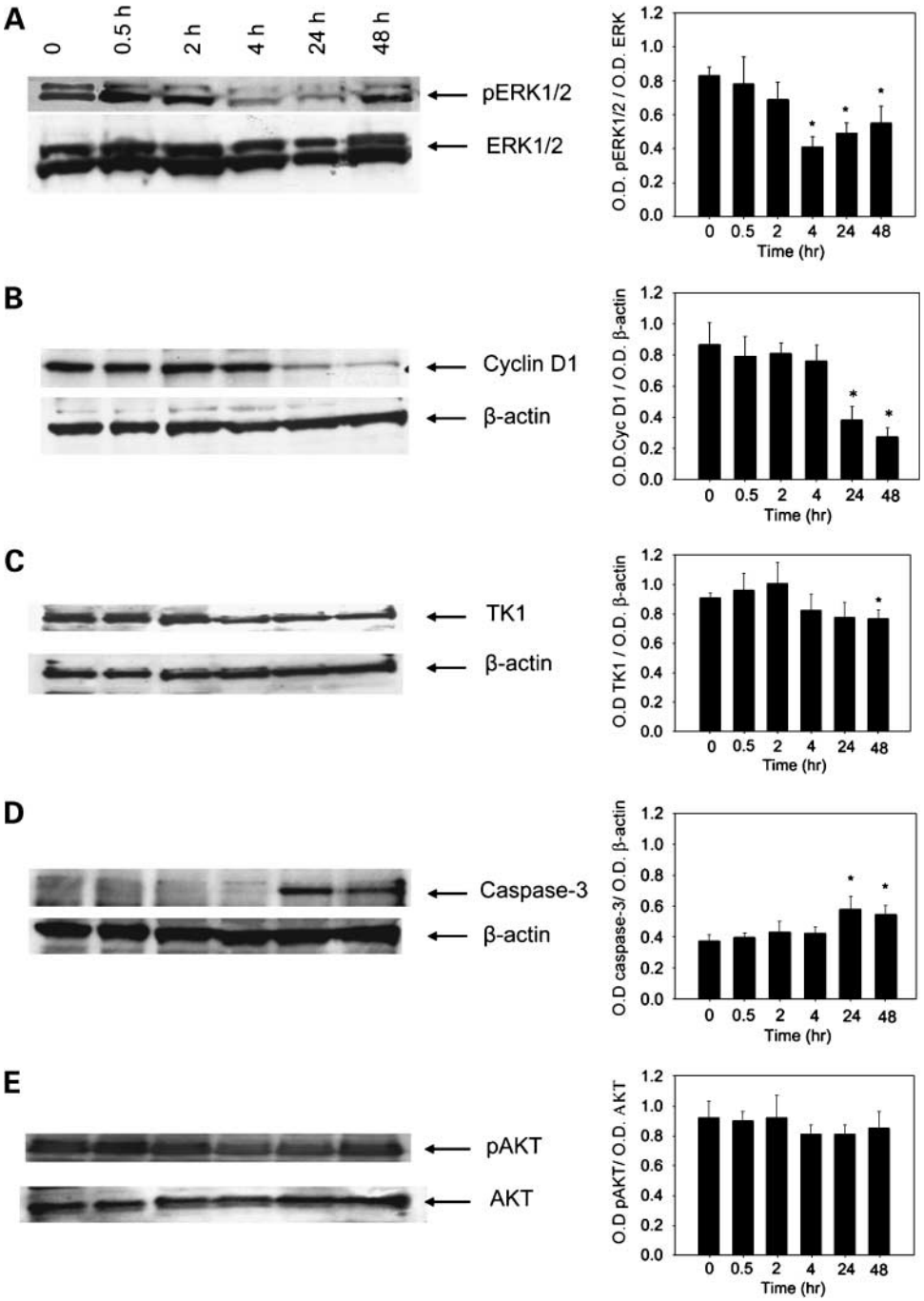


**Figure 1.** The effect of PD0325901 on protein expression levels as determined by Western blot in SKMEL-28 cells. Typical Western blots showing the time course of drug effect on pERK 1/2 ($Thr^{202}/Thr^{204}$; **A**), cyclin D1 (**B**), TK1 (**C**), cleaved caspase-3 (**D**), and pAKT (**E**) proteins together with corresponding total ERK1/2 levels and β-actin (loading control). The cells were treated with 1.0 μmol/L of PD0325901 for 0.5, 2, 4, 24, and 48 h prior to analysis. A summary of the densitometry measurements are also shown in the respective panels. *Columns,* mean; *bars,* SE ($n = 3$).

measured continuously using a caliper and tumor volumes were calculated by the equation: volume = $(\pi/6) \times a \times b \times c$, where $a$, $b$, and $c$ represent three orthogonal axes of the tumor. Mice were used when their tumors reached ~100 $mm^3$. Size-matched tumor-bearing mice were randomized to receive 25 mg/kg (0.005 mL/g mouse) of PD0325901 or vehicle (0.5% hydroxypropyl methylcellulose plus 0.2% Tween 80) daily by oral gavage. [$^{18}$F]FLT-PET scanning was done at ~25 hours after commencing treatment (i.e., after two doses with the second dose given 1 hour before scanning) or after 10 daily treatments (again with the last dose given 1 hour before scanning). After imaging, one part of the tumor was snap-frozen in liquid nitrogen and stored at −80°C; the other part was fixed in formal saline.

### PET Imaging Studies

Dynamic [$^{18}$F]FLT-PET studies were carried out on a dedicated small animal PET scanner, quad-HIDAC (Oxford Positron Systems). The features of this instrument have been previously described (19). Scanning was done using a previously reported protocol (13). Dynamic scans were acquired in list-mode format over a 60-min period.

### Image Analysis and Quantification

Cumulative images comprising of 30 to 60 min of the dynamic data were used for visualization of radiotracer uptake and to draw regions of interest. Regions of interest were defined on five tumor and five heart-slices (each 0.5 mm in thickness). Dynamic data from these slices were averaged for each tissue and at each of the 19 time points to obtain time versus radioactivity curves for these tissues. Tumor radioactivity was corrected for physical decay and normalized to that of heart to obtain a standardized uptake value (NUV). The NUV at 60 min postinjection ($NUV_{60}$) was used for comparisons; to improve signal-to-noise ratio, $NUV_{max}$ was also calculated in a similar manner as $NUV_{60}$ except that maximal voxel radioactivities for each tumors' region of interest were used. The area under the NUV curve (AUC) was calculated as the integral of NUV from 0 to 60 min. The fractional retention of tracer (FRT) at 60 min relative to that at 1.5 min was also calculated (13).

### Immunohistochemical Analysis of Proliferation

PD0325901- and vehicle-treated tumors ($n$ = 4 each) were excised after imaging, fixed in formalin, embedded in paraffin, and cut into 5.0-μm sections. The degree of tumor proliferation was assessed in tumor sections as previously described (13). For each tumor section, the total number of Ki67-positive brown-stained cells and hematoxylin-stained cells were counted in 16 randomly selected fields of view using an Olympus BX51 microscope (Olympus UK, Ltd.) at ×400 magnification. The Ki67 labeling index ($LI_{Ki67}$) was calculated using the equation $LI_{Ki67}$ = [Ki67-positive cells / (total cells)] × 100%.

### Double-Labeled Immunofluorescence

Deparaffinized sections were fixed in 3% to 4% paraformaldehyde in PBS (pH 7.4) for 15 min at room temperature and permeabilized for 20 min with PBS containing 0.25% Triton X-100 at room temperature, and then washed thrice with PBS for 5 min. After washing, the sections were blocked with 1% bovine serum albumin in PBS containing 0.25% Triton X-100 for 30 min at room temperature. Subsequently, they were incubated with a mixture of pERK1/2 antibodies (1:100; Cell Signaling) and Ki67 antibodies (1:100; Dako) diluted in 1% bovine serum albumin in PBS containing 0.25% Triton X-100 for 16 h at 4°C. After washing (five times) with PBS, the sections were incubated for 1 hour at room temperature with a mixture of Alexa Fluor 488–conjugated goat anti-rabbit antibodies (Invitrogen) diluted 1:400 and Alexa Fluor 594–conjugated goat anti-mouse antibodies (Invitrogen) diluted 1:400 in 1% bovine serum albumin. The sections were then washed five times with PBS and mounted with gel mount containing 4′,6-diamidino-2-phenylindole (Invitrogen). Specimens were examined for fluorescence with an Olympus BX51 microscope (Olympus); the results were compared with H&E staining.

### Statistical Analysis

Data were expressed as mean ± SE. Statistical analyses were done using the software GraphPad Prism, version 3.03 (GraphPad). Group comparisons were assessed using the nonparametric Mann-Whitney test. Correlations between tumor radiotracer levels and $LI_{Ki67}$ were determined (Pearson correlation). Two-tailed $P \leq 0.05$ were considered significant.

## Results

### Suppression of ERK1/2 Phosphorylation by PD0325901 in SKMEL-28 cells

The phosphorylation of ERK1/2 protein (44/42 kDa) was detected by Western blotting. A time-dependent reduction in pERK1/2 was induced by 1 μmol/L of PD0325901 (Fig. 1A). Maximum and significant reduction of pERK1/2 was observed at 4 hours compared with vehicle control ($P$ = 0.03) after treating cells with PD0325901, and there was partial recovery of the protein at 24 and 48 hours after treatment ($P$ = 0.05). The observed change in pERK1/2 expression was not accompanied by changes in total ERK1/2 expression, indicating that the reduction in ERK1/2 phosphorylation by PD0325901 was not due to a depletion of the protein.

### PD0325901 Inhibits Cyclin D1 and TK1 Protein Expression, and Induces the Cleavage of Caspase-3 in SKMEL-28 Cells

In most cell types, sustained activation of MAPK signaling pathway leads to activation of the cyclin D–cdk4 complex to modulate cell proliferation (9, 20, 21). PD0325901 (1 μmol/L) reduced cyclin D1 protein expression (Fig. 1B) at 24 and 48 hours after treatment compared with vehicle control ($P$ = 0.03). Compared with pERK1/2 (Fig. 1B), the recovery of cyclin D1 was slower. Like cyclin D1 protein, TK1 protein levels decreased with PD0325901 treatment in a time-dependent manner (Fig. 1C); the decrease in TK1 expression following drug treatment was also slower than those for pERK1/2, with maximum reduction at 48 hours posttreatment ($P$ = 0.03). The drug caused a small but significant induction of caspase-3

cleavage at 24 and 48 hours compared with vehicle-treated cells (Fig. 1D). Lastly, as a negative control, we examined the effect of PD0325901 on pAKT levels. No consistent time-related alterations in pAKT levels were observed (Fig. 1E) at the drug concentration used (1 μmol/L).

**P0325901 Inhibits TK1 and Cyclin D1 mRNA Expression**

The mRNA levels of TK1, cyclin D1, and ELK in SKMEL-28 cells were all significantly down-regulated within hours following treatment with 1 μmol/L of PD0325901 compared with vehicle control (Fig. 2A–C). Significant inhibition of cyclin D1 and TK1 mRNA was detectable at the earliest time point (4 hours; $P = 0.001$ and 0.03, respectively) and persisted for the duration of the study (48 hours). The nuclear transcription factor ELK, which is a direct downstream target of pERK1/2 (22, 23) was also down-regulated at 4 hours in response to PD0325901. The recovery kinetics of ELK were, however, more rapid than those for cyclin D1 and TK1. Of note, PD0325901 also induced a significant $G_1$ arrest at the lowest dose concentration studied (0.01 μmol/L): 81.6 ± 0.8% of cells were in $G_1$ phase compared with 56.8 ± 4.4% for vehicle control ($P = 0.03$; Supplementary Fig. S1).[6]

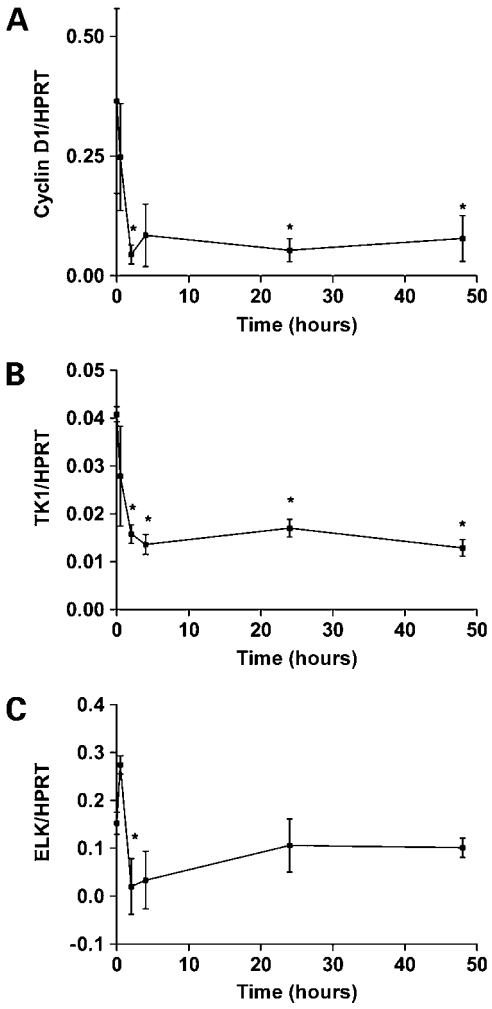


**Figure 2.** Effect of PD0325901 on cyclin D1 (**A**), TK1 (**B**), and ELK (**C**) mRNA levels in SKMEL-28 cells *in vitro* analyzed by quantitative real-time PCR. *Points,* mean; *bars,* SE ($n = 3$). mRNA levels were normalized to that of the housekeeping gene *HPRT* and expressed as a ratio.

**Effect of PD0325901 on SKMEL-28 and HCT116 Tumor Growth**

For both tumor types, tumor volumes were not significantly reduced at day 1 following PD0325901 (25 mg/kg) treatment (Fig. 3A). In SKMEL-28, tumor volume changed from 168.0 ± 38.5 $mm^3$ (pretreatment group) to 181.2 ± 28.8 $mm^3$ and 248.0 ± 36.9 $mm^3$ at days 1 and 10, respectively, following treatment with vehicle. In contrast, tumor shrinkage was observed after daily treatment with PD0325901 (25 mg/kg) to 135.8 ± 19.0 and 43.2 ± 16.3 $mm^3$ ($P = 0.05$), at days 1 and 10, respectively. HCT116 tumor volumes showed a rapid increase in the vehicle-treated group from 106.670 ± 15.70 $mm^3$ (pretreatment group) to 136.7 ± 38.6 $mm^3$ and 542.3 ± 115.0 $mm^3$ at days 1 and 10, respectively. In contrast, tumor stasis was seen with PD0325901 treatment; tumor volumes were 82.9 ± 18.9 and 128.5 ± 29.3 $mm^3$ ($P = 0.05$) at days 1 and 10, respectively. No significant changes in mouse body weights were observed with drug treatment (data not shown).

**PD0325901 Inhibits the Kinetics of [$^{18}$F]FLT Retention in Both SKMEL-28 and HCT116 Xenografts**

Typical (0.5 mm) transverse PET image slices demonstrating the accumulation of [$^{18}$F]FLT in tumor regions are shown in Fig. 3B. Qualitative reductions in radiotracer localization were observed in the tumors of PD0325901-treated mice. Whereas NUV increased over time in vehicle-treated tumors, PD0325901 induced significant reductions in [$^{18}$F]FLT uptake compared with vehicle treatment (Fig. 3C and D). Summary data are presented in Table 1 and show that although the $NUV_{60}$, $NUV_{max}$, AUC, and FRT were unchanged in the vehicle control groups, all the variables were significantly lower in the PD0325901-treated groups compared with corresponding vehicle-treated groups. FRT in HCT116 tumor decreased but the decrease was not statistically significant.

***In vivo* Activity of PD0325901 is Associated with Reductions in Ki67 Labeling and TK1 Protein Levels in SKMEL-28 and HCT116 Xenografts**

Significant changes in $LI_{Ki67}$ were seen after 1 and 10 days of drug treatment in SKMEL-28 xenografts ($P = 0.03$ for both; Fig. 4A and B). Similarly, $LI_{Ki67}$ was lower in HCT116 tumors after 10 days of drug treatment ($P = 0.05$; Fig. 4C). In this tumor, changes in $LI_{Ki67}$ at day 1 were not statistically significant. All tumor data (SKMEL-28 and HCT116) were combined for the assessment of the degree of association between tumor [$^{18}$F]FLT kinetic variables and cell proliferation. The correlation coefficient ($r$) between $LI_{Ki67}$ and $NUV_{60}$ was 0.630 ($P = 0.001$), and that for $LI_{Ki67}$ versus FRT was 0.596 ($P = 0.003$); $LI_{Ki67}$ versus AUC was also significant ($r = 0.647$; $P = 0.002$). There was also a significant correlation between [$^{18}$F]FLT kinetic variables and tumor TK1 expression: $r$ was 0.518 ($P = 0.002$), 0.423 ($P = 0.015$), and 0.480 ($P = 0.005$) for $NUV_{60}$, AUC, and FRT, respectively.

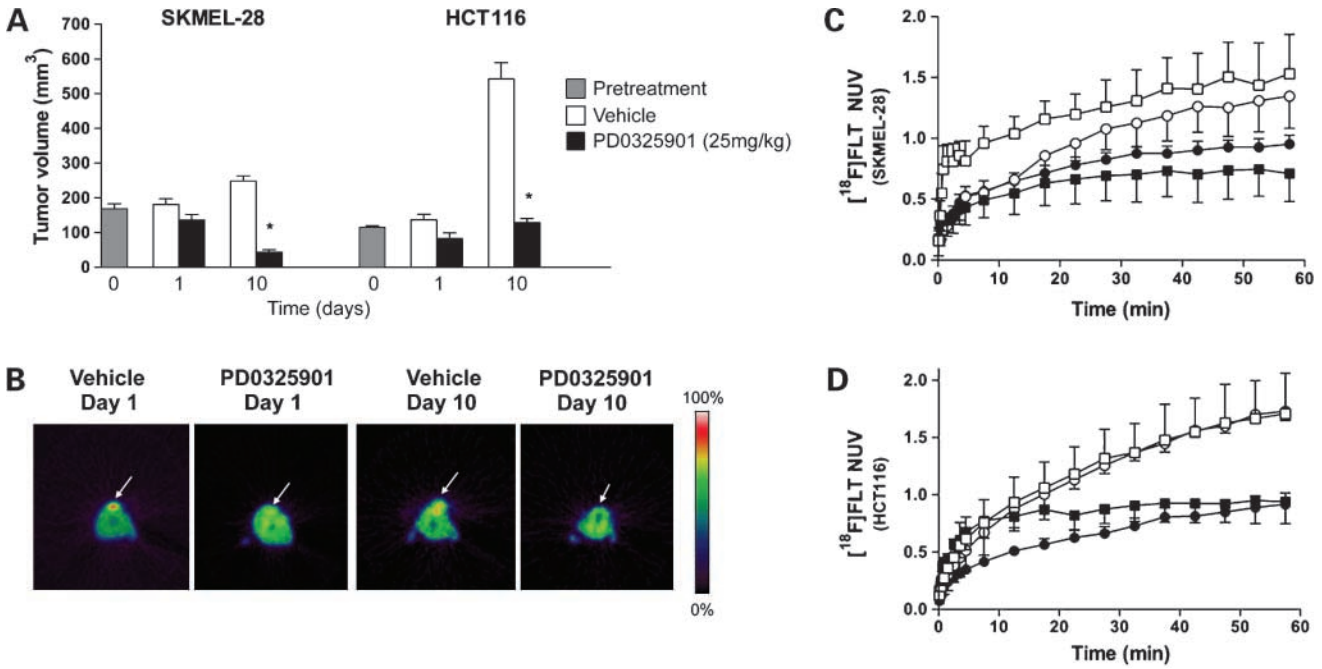


**Figure 3.** The effects of PD0325901 on tumor growth and [$^{18}$F]FLT uptake. **A,** growth curves for SKMEL-28 and HCT116 tumor xenografts. Mice were treated with vehicle (0.5% hydroxypropyl methylcellulose plus 0.2% Tween 80) or PD0352901 formulated in vehicle and given at 25 mg/kg daily by oral gavage for 10 d commencing when tumors reached a volume of between 100 and 150 mm$^3$. *Columns,* mean; *bars,* SE ($n$ = 4 mice per group). **B,** typical transverse (0.5 mm) [$^{18}$F]FLT-PET images of SKMEL-28 tumor-bearing mice after 1 and 10 d of vehicle or PD0352901 treatment (25 mg/kg; oral gavage). For visualization, 30 to 60 min summed image data are displayed. *Arrows,* tumors. Also note color bar. **C,** [$^{18}$F]FLT-PET time versus radioactivity curves for the different treatment groups in SKMEL-28 tumors and for HCT116 tumors (**D**). The treatment groups were day 1 after vehicle (□), day 1 after PD0325901 (●), 10 d after vehicle (○), and 10 d after PD0325901 (■). For each tumor, the NUV at each of 19 time points was determined. *Points,* mean NUV; *bars,* SE ($n$ = 4 mice per group); for clarity, top or bottom bars are shown.

Significant reductions in pERK1/2, cyclin D1, and TK1 protein levels were observed after drug treatment *in vivo* compared with vehicle controls (Supplementary Table S2). ATP levels were also significantly lower after 1 and 10 days of drug treatment compared with controls (Supplementary Table S2).[6]

### Double-Immunofluorescence Detection of pERK1/2 and Ki67 in SKMEL-28 Tumors

The coexpression of Ki67 and pERK1/2 in SKMEL-28 tumor sections is shown in Fig. 5. Whereas Ki67-positivity (*red*) was confined to the nucleus pERK1/2-positivity (*green*) was both nuclear and cytoplasmic. Coexpression

**Table 1. Summary of pharmacokinetic PET variables for [$^{18}$F]FLT obtained from the time versus radioactivity curves in vehicle-treated and PD0325901-treated tumor-bearing mice**

| | Vehicle, day 1 | PD0325901 (25 mg/kg), day 1 | Vehicle, day 10 | PD0325901 (25 mg/kg), day 10 |
|---|---|---|---|---|
| (A) SKMEL-28 tumor | | | | |
| $NUV_{60}$ | 1.52 ± 0.32 | 0.72 ± 0.23* | 1.38 ± 0.26 | 0.93 ± 0.1† |
| $NUV_{max}$ | 1.81 ± 0.18 | 1.23 ± 0.10† | 2.07 ± 0.40 | 1.08 ± 0.14† |
| AUC | 60.58 ± 9.46 | 38.76 ± 13.80* | 72.43 ± 13.87 | 49.02 ± 13.72† |
| $FRT_{1.5/60}$ | 3.27 ± 0.64 | 2.69 ± 1.01* | 3.76 ± 0.87 | 2.52 ± 0.24† |
| (B) HCT116 tumor | | | | |
| $NUV_{60}$ | 1.70 ± 0.35 | 0.93 ± 0.19† | 1.73 ± 0.08 | 0.91 ± 0.1† |
| $NUV_{max}$ | 2.30 ± 0.84 | 1.88 ± 0.36* | 1.97 ± 0.13 | 1.00 ± 0.03† |
| AUC | 70.68 ± 16.65 | 51.11 ± 7.74† | 73.57 ± 3.79 | 40.21 ± 3.22† |
| $FRT_{1.5/60}$ | 3.27 ± 0.74 | 2.72 ± 0.88 | 4.11 ± 2.04 | 3.25 ± 0.97 |

NOTE: Data are the mean ± SE ($n$ = 4).
Abbreviations: $NUV_{60}$, normalized uptake value at 60 min. $NUV_{max}$, normalized uptake values determined from voxels with the highest radioactivity. AUC, area under the curve. FRT, fractional retention of [$^{18}$F]radioactivity at 60 min relative to 1.5 min.
*Significantly different from vehicle ($P$ = 0.045).
†Significantly different from vehicle ($P$ = 0.03).

of pERK1/2-positive cells and Ki67-positive cells was indicated by the yellow fluorescence. In vehicle-treated tumors, almost all the pERK1/2-positive cells were also Ki67-positive (Fig. 5A). The coexpression of pERK1/2 and Ki67 was detectable after 1 day of PD0325901 treatment but the total number of (*yellow*) cells within the tumor mass had decreased (Fig. 5B). At 10 days after PD0325901 treatment, Ki67 nuclear staining was barely detectable. In contrast, there were pockets of cells with pERK1/2 cytoplasmic staining; no pERK1/2 nuclear staining was detectable (Fig. 5C).

## Discussion

We have shown that the reduction in cell proliferation induced by PD0325901 is detectable by [$^{18}$F]FLT-PET variables $NUV_{60}$, $NUV_{max}$, AUC, and FRT. The MAPK signal transduction pathway is an attractive target for therapeutic intervention because several cancers harbor amplifications and mutations of genes within the pathway leading to constitutive activation of downstream effectors. In preclinical models, MEK1/2 inhibitors showed activity in tumors harboring mutations in *BRAF* or *RAS* (6, 9). In recent phase I and II clinical trials of these inhibitors, stable disease was observed as the best clinical outcome despite significant reductions in pERK1/2 levels (5, 7, 8). Smalley and coworkers (10) recently showed that drug-induced reductions in the proliferation marker Ki67 correlated better with the growth-inhibitory activity of MEK1/2 inhibitors than changes in pERK1/2 and suggested the use of this biomarker in addition to pERK1/2 in future trials of MEK1/2 inhibitors. Because a noninvasive imaging biomarker may be more desirable than a histologic biomarker such as Ki67, we investigated if and how [$^{18}$F]FLT-PET imaging of cell proliferation could fulfill this role. Indeed, Solit and coworkers have recently shown the advantage of [$^{18}$F]FLT-PET over [$^{18}$F]fluorodeoxyglucose-PET in monitoring the response to the MEK1/2 inhibitor, PD0325901 (16).

[$^{18}$F]FLT uptake into tumors is a function of the levels of the TK1 enzyme and of the cofactor ATP (11, 12). Studies in xenograft models (13–15, 19) and in human tumors (24, 25) have shown strong correlations between [$^{18}$F]FLT uptake and $LI_{Ki67}$. *In vitro* studies in SKMEL-28 cells showed that mRNA and protein levels of TK1 were rapidly decreased after MEK1/2 inhibition by PD0325901 (Figs. 1 and 2). These findings, together with the strong $G_1$ arrest in treated cells, suggested that [$^{18}$F]FLT might be a useful biomarker for imaging MEK1/2 inhibition by PD0325901. The time course studies after single drug dosing indicated that recovery of pERK1/2 and ELK was more rapid than that for the protein/mRNA for cyclin D1 and TK1. These findings indicate that a TK1-based imaging probe will not measure MEK1/2 activity directly but rather downstream effects of MEK1/2 inhibition, the kinetics of which may be somewhat different from direct target activity.

Treatment of SKMEL-28 and HCT116 tumors led to reductions in [$^{18}$F]FLT uptake in drug-treated mice compared

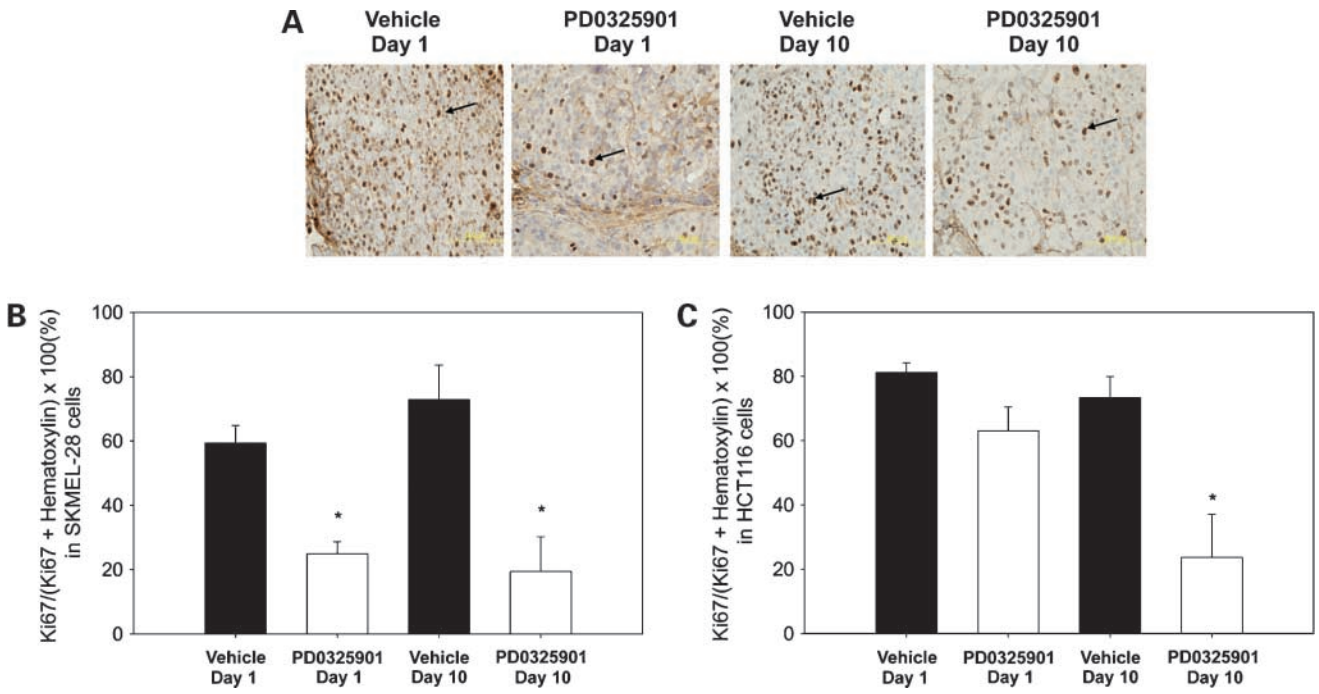


**Figure 4.** Effect of PD0352901 on $LI_{Ki67}$. **A,** typical histologic sections of SKMEL-28 immunostained with Ki67 antibody and counterstained with hematoxylin. Four treatment groups were examined (day 1 after vehicle, day 1 after PD0325901, 10 d after vehicle, and 10 days after PD0325901). *Arrows,* Ki67-positive nuclei (*brown*). Magnification, ×400. **B,** summary of tumor $LI_{Ki67}$ for the different SKMEL-28 treatment groups. **C,** summary of tumor $LI_{Ki67}$ for the different HCT116 treatment groups. *Columns,* mean $LI_{Ki67}$; *bars,* SE ($n$ = 4 tumors).

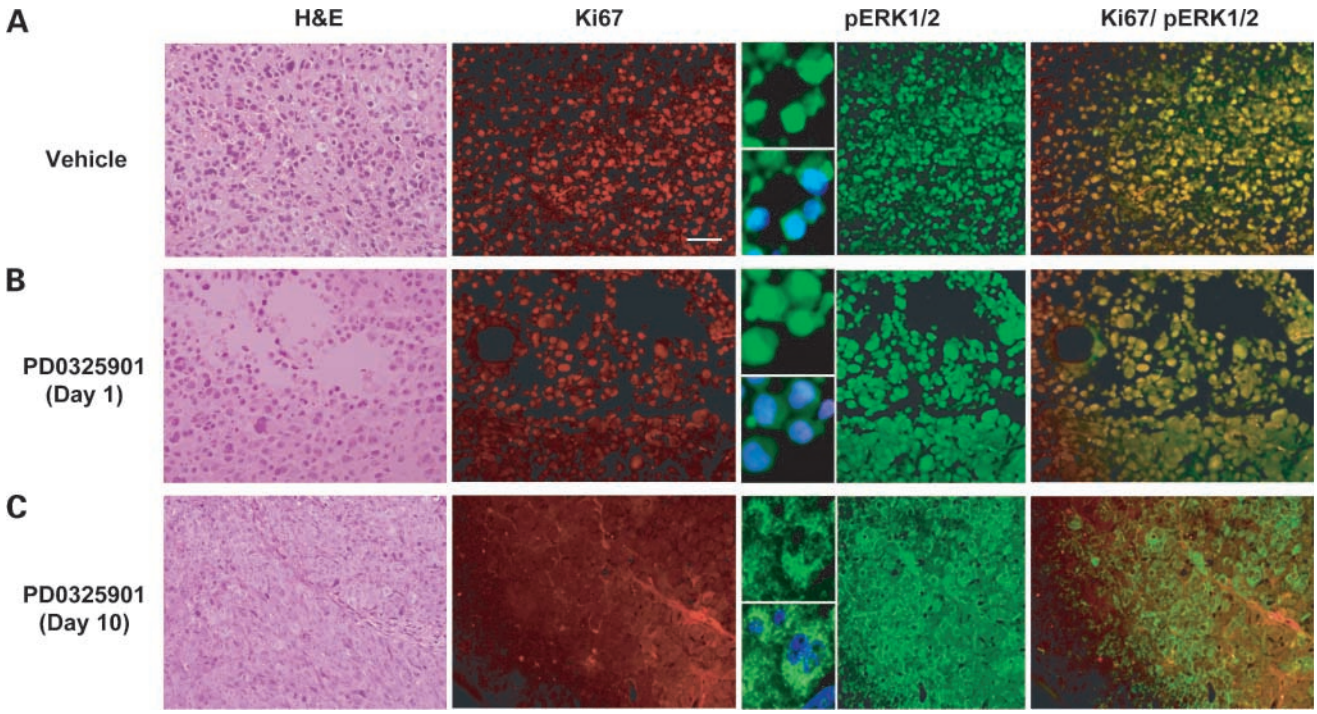


**Figure 5.** Double-labeled immunofluorescence for Ki67 (*red*) and pERK1/2 (*green*) in SKMEL-28 tumor sections. Double-stained cells (*yellow*). Corresponding H&E staining has been included. Sections (magnification, ×400) are illustrated for vehicle-treated tumors (**A**); PD0325901 day 1 treatment (**B**); and PD0325901 day 10 treatment (**C**); *bars,* 200 μm. *Insets,* expanded views of tumor cells with and without nuclear 4′,6-diamidino-2-phenylindole counterstaining. At day 10, pERK was expressed only within the cytoplasm.

with vehicle controls. In contrast with previous reports suggesting that cells with *K-RAS* mutation are unresponsive to PD0325901 (9), we saw [$^{18}$F]FLT responses in the HCT116 tumor model. In these imaging studies, baseline radiotracer uptake should be assumed to be similar to that in day 1 vehicle-treated mice. In previous [$^{18}$F]FLT imaging studies in RIF-1 (14) and IGROV-1 (15), we found no differences between radiotracer uptake/biochemical variables in size-matched untreated tumors versus tumors treated with vehicle for 1 day, and therefore, as with recent studies, we compared day 1 vehicle-treated to day 1 drug-treated groups (13, 26). The lower [$^{18}$F]FLT uptake in drug-treated compared with vehicle-treated tumors at day 1, therefore, supports the assertion that [$^{18}$F]FLT-PET imaging can be used to measure early changes in proliferation following PD0325901 treatment. Of interest, where drug effects on proliferation are delayed, we see no early changes in tumor [$^{18}$F]FLT uptake, as shown in a recent study (26). The study design reported here is different from one that will be used clinically, i.e., pretreatment scans followed by posttreatment scans in the same patient, but is useful in that it permits direct comparison of the imaging end point to tumor biochemistry in individual animal tumors.

In general, the reductions in [$^{18}$F]FLT kinetic variables were associated with changes in $LI_{Ki67}$ ($r \geq 0.6$; $P \geq 0.003$) suggesting that [$^{18}$F]FLT-PET imaging may be useful as a marker of changes in cell proliferation following MEK1/2 inhibition. This is in agreement with previous studies with other drugs in which good correlations were seen between [$^{18}$F]FLT uptake variables and $LI_{Ki67}$ (13–15). There were significant differences in $LI_{Ki67}$ between drug-treated animals and their respective vehicle control groups for SKMEL-28 (days 1 and 10) and HCT116 (day 10). Changes in $LI_{Ki67}$ did not, however, discriminate between tumor shrinkage in a SKMEL-28 model and modest growth inhibition in a HCT116 model, a finding that could be explained at least in part by the very different growth rates of the two tumor types. Also of note, a direct relationship between HCT116 tumor volume and [$^{18}$F]FLT uptake was not seen. This finding is not dissimilar from our previous observations in mice (13–15, 19) and humans (27), and supports the notion that changes in proliferation are more sensitive and precede tumor size changes. The group-averaged PET kinetic variables may, however, have been influenced by spatial differences in radiotracer uptake, which could have introduced errors in averaging of [$^{18}$F]FLT within regions of interest. For instance, although the group-averaged $NUV_{60}$ was unchanged between days 1 and 10 for drug-treated SKMEL-28, $LI_{Ki67}$ decreased. The reduction of $NUV_{max}$ was more consistent with changes in $LI_{Ki67}$ than in $NUV_{60}$, presumably because of the lower signal-to-noise characteristics of the former. The reduction in PET variables was consistent with changes in TK1 enzyme and ATP levels *in vivo*.

An important aspect of this work was to investigate, with a dynamic imaging protocol, if different [$^{18}$F]FLT-PET variables change differently with drug treatment. In general, all four [$^{18}$F]FLT-PET variables decreased after drug treatment with slightly different levels of change at the two time points studied (Table 1A and B). Reductions in all four imaging variables implied that the drug-induced effects detectable by [$^{18}$F]FLT-PET could not simply be attributed to modulation of, for instance, tumor perfusion which may accompany the biological activity of some kinase inhibitors. This finding also implies that the semiquantitative imaging variable—standardized uptake value—often employed in clinical PET studies may be a useful variable in the clinical pharmacodynamic assessment of MEK1/2 inhibition by PD0325901 and potentially other MEK1/2 inhibitors.

A more detailed study to link the effect of PD0325901 on pERK1/2 to changes in Ki67 showed a time-dependent reduction in both pERK1/2 and Ki67 expression by PD0325901. The presence of Ki67-negative pERK1/2 (cytoplasmic)–positive cells in tumors treated with PD0325901 for 10 days is consistent with the need for pERK1/2 to translocate to the nucleus in order to affect transcription (20–23). Analysis of tumor material by Western blotting does not discriminate cytoplasmic from nuclear pERK1/2 levels. Thus, assuming that reduction in nuclear pERK1/2 (Fig. 5C) is a major effect of this drug, small changes in pERK1/2 detectable by Western blot could be associated with large changes in Ki67. Regarding other mechanisms of drug response, an increase in sub-$G_0$ (apoptotic) cells and cleaved caspase-3 activities were seen in treated cells *in vitro*, indicating that the apoptotic pathway is active with PD0325901 treatment. The level of apoptosis was, however, distinctly low in both tumor types, indicating that apoptosis was not a major mechanism of tumor growth inhibition. An important consideration for pharmacodynamic assessment of pathway-specific drugs is that the concentration of drug required to inhibit pathway activity may be insufficient to inhibit downstream signaling irrespective of upstream mutational status. The use of end points, such as [$^{18}$F]FLT-PET, that report on growth inhibition should be considered alongside end points which report on target activity.

In summary, [$^{18}$F]FLT-PET is a sensitive imaging biomarker for detecting the antiproliferative effect of MEK1/2 inhibition by PD0325901; it does not directly measure MEK1/2 activity. This imaging method may be useful in the clinical development of PD0325901 and other inhibitors of the MAPK pathway.

## Disclosure of Potential Conflicts of Interest

No potential conflicts of interest were disclosed.

### Acknowledgments

We thank the members of the Molecular Therapy group, Imperial College London, for critical reading and discussion of the manuscript, and the staff of the Biological Imaging Centre of Imperial College for support with imaging studies.

### References

1. Hoshino R, Chatani Y, Yamori T, et al. Constitutive activation of the 41-/43-kDa mitogen-activated protein kinase signaling pathway in human tumors. Oncogene 1999;18:813–22.

2. Davies H, Bignell GR, Cox C, et al. Mutations of the BRAF gene in human cancer. Nature 2002;417:949–54.

3. Wellbrock C, Ogilvie L, Hedley D, et al. V599EB-RAF is an oncogene in melanocytes. Cancer Res 2004;64:2338–42.

4. Smith G, Carey FA, Beattie J, et al. Mutations in APC, Kirsten-ras, and p53-alternative genetic pathways to colorectal cancer. Proc Natl Acad Sci U S A 2002;99:9433–8.

5. Adjei AA, Cohen RB, Franklin W, et al. Phase I pharmacokinetic and pharmacodynamic study of the oral, small-molecule mitogen-activated protein kinase kinase 1/2 inhibitor AZD6244 (ARRY-142886) in patients with advanced cancers. J Clin Oncol 2008;26:2139–46.

6. Davies BR, Logie A, McKay JS, et al. AZD6244 (ARRY-142886), a potent inhibitor of mitogen-activated protein kinase/extracellular signal-regulated kinase kinase 1/2 kinases: mechanism of action *in vivo*, pharmacokinetic/pharmacodynamic relationship, and potential for combination in preclinical models. Mol Cancer Ther 2007;6:2209–19.

7. Lorusso PM, Adjei AA, Varterasian M, et al. Phase I and pharmacodynamic study of the oral MEK inhibitor CI-1040 in patients with advanced malignancies. J Clin Oncol 2005;23:5281–93.

8. Rinehart J, Adjei AA, Lorusso PM, et al. Multicenter phase II study of the oral MEK inhibitor, CI-1040, in patients with advanced non-small cell lung, breast, colon, and pancreatic cancer. J Clin Oncol 2004;22:4456–62.

9. Solit DB, Garraway LA, Pratilas CA, et al. BRAF mutation predicts sensitivity to MEK inhibition. Nature 2006;439:358–62.

10. Smalley KS, Contractor R, Haass NK, et al. Ki67 expression levels are a better marker of reduced melanoma growth following MEK inhibitor treatment than phospho-ERK levels. Br J Cancer 2007;96:445–9.

11. Barthel H, Perumal M, Latigo J, et al. The uptake of 3′-deoxy-3′-[18F]fluorothymidine into L5178Y tumours *in vivo* is dependent on thymidine kinase 1 protein levels. Eur J Nucl Med Mol Imaging 2005;32:257–63.

12. Rasey JS, Grierson JR, Wiens LW, Kolb PD, Schwartz JL. Validation of FLT uptake as a measure of thymidine kinase-1 activity in A549 carcinoma cells. J Nucl Med 2002;43:1210–7.

13. Leyton J, Alao JP, Da Costa M, et al. *In vivo* biological activity of the histone deacetylase inhibitor LAQ824 is detectable with 3′-deoxy-3′-[18F]fluorothymidine positron emission tomography. Cancer Res 2006;66:7621–9.

14. Leyton J, Latigo JR, Perumal M, et al. Early detection of tumor response to chemotherapy by 3′-deoxy-3′-[18F]fluorothymidine positron emission tomography: the effect of cisplatin on a fibrosarcoma tumor model *in vivo*. Cancer Res 2005;65:4202–10.

15. Leyton J, Lockley M, Aerts JL, et al. Quantifying the activity of adenoviral E1A CR2 deletion mutants using renilla luciferase bioluminescence and 3′-deoxy-3′-[18F]fluorothymidine positron emission tomography imaging. Cancer Res 2006;66:9178–85.

16. Solit DB, Santos E, Pratilas CA, et al. 3′-Deoxy-3′-[18F]fluorothymidine positron emission tomography is a sensitive method for imaging the response of BRAF-dependent tumors to MEK inhibition. Cancer Res 2007;67:11463–9.

17. Oh SJ, Mosdzianowski C, Chi DY, et al. Fully automated synthesis system of 3′-deoxy-3′-[18F]fluorothymidine. Nucl Med Biol 2004;31:803–9.

18. Workman P, Balmain A, Hickman JA, et al. UKCCCR guidelines for the welfare of animals in experimental neoplasia. Lab Anim 1988;22:195–201.

19. Barthel H, Cleij MC, Collingridge DR, et al. 3′-Deoxy-3′-[18F]fluorothymidine as a new marker for monitoring tumor response to antiproliferative therapy *in vivo* with positron emission tomography. Cancer Res 2003;63:3791–8.

20. Balmanno K, Cook SJ. Sustained MAP kinase activation is required for the expression of cyclin D1, p21Cip1 and a subset of AP-1 proteins in CCL39 cells. Oncogene 1999;18:3085–97.

21. Weber JD, Raben DM, Phillips PJ, Baldassare JJ. Sustained activation of extracellular-signal-regulated kinase 1 (ERK1) is required for the

continued expression of cyclin D1 in G1 phase. Biochem J 1997;326:61–8.

**22.** Cruzalegui FH, Cano E, Treisman R. ERK activation induces phosphorylation of Elk-1 at multiple S/T-P motifs to high stoichiometry. Oncogene 1999;18:7948–57.

**23.** Galetic I, Maira SM, Andjelkovic M, Hemmings BA. Negative regulation of ERK and Elk by protein kinase B modulates c-Fos transcription. J Biol Chem 2003;278:4416–23.

**24.** Buck AK, Halter G, Schirrmeister H, et al. Imaging proliferation in lung tumors with PET: 18F-FLT versus 18F-FDG. J Nucl Med 2003;44:1426–31.

**25.** Kenny LM, Vigushin DM, Al-Nahhas A, et al. Quantification of cellular proliferation in tumor and normal tissues of patients with breast cancer by [18F]fluorothymidine-positron emission tomography imaging: evaluation of analytical methods. Cancer Res 2005;65:10104–12.

**26.** Chan F, Sun C, Perumal M, et al. Mechanism of action of the Aurora kinase inhibitor CCT129202 and *in vivo* quantification of biological activity. Mol Cancer Ther 2007;6:3147–57.

**27.** Kenny L, Coombes RC, Vigushin DM, et al. Imaging early changes in proliferation at 1 week post chemotherapy: a pilot study in breast cancer patients with 3′-deoxy-3′-[18F]fluorothymidine positron emission tomography. Eur J Nucl Med Mol Imaging 2007;34:1339–47.

Molecular Cancer Therapeutics

# Noninvasive imaging of cell proliferation following mitogenic extracellular kinase inhibition by PD0325901

Julius Leyton, Graham Smith, Mark Lees, et al.

*Mol Cancer Ther* 2008;7:3112-3121.